

Article

Different Toppling Bank Slope Failures under Hydrodynamic Action during Impoundment of the Miaowei Hydropower Station Reservoir

Zhigang Shan ¹, Jingqing Lv ², Faming Zhang ^{3,*}, Liang Chen ², Fei Yin ² and Menglong Dong ³

¹ PowerChina Huadong Engineering Corporation Limited, Hangzhou 311122, China; shan_zg@hdec.com

² Huadong Engineering (Fujian) Corporation Limited, Fuzhou 350000, China; lv_jq@ecidi.com (J.L.); chen_l20@hdec.com (L.C.); yin_f@ecidi.com (F.Y.)

³ Institute of Engineering Geology and Geohazards, Hohai University, Nanjing 210098, China; dongml@hhu.edu.cn

* Correspondence: zhangfm@hhu.edu.cn; Tel.: +86-13770671695

Abstract: Toppling is a common deformation and failure phenomenon in the reservoir bank slopes of hydropower projects. This paper studies the genesis and evolution of different toppling bodies during water impoundment at the Miaowei Hydropower Station Reservoir on the Lancang River in southwest China. Toppling properties were determined and second failure characteristics analyzed in different reservoir impoundment stages. Different degrees of toppling deformation were primarily affected by the transverse bending stress, while the regional tectonic stress has been shown to have a significant effect on the transverse bending of the rock layers. Combined with the on-site investigation and monitoring results, the failure mechanisms of the different toppling deformation bodies were analyzed. The second failure of the toppling rock mass caused by the reservoir impoundment process is mainly the hydrodynamic splitting along fractures, wave impactation and softening on the slope foot. The transverse bending effect of gravity is transmitted upward through joint misalignment, rotation and slip, accelerating the speed of secondary toppling failure and forming a compression-shear failure along the toppling tension crack. A model to predict the scope and time of failure in the toppling deformation banks under the action of reservoir hydrodynamics was proposed.

Keywords: toppling deformation rock mass; hydrodynamic action; compression-shear failure; failure prediction model; secondary toppling failure



Citation: Shan, Z.; Lv, J.; Zhang, F.; Chen, L.; Yin, F.; Dong, M. Different Toppling Bank Slope Failures under Hydrodynamic Action during Impoundment of the Miaowei Hydropower Station Reservoir. *Water* **2022**, *14*, 2126. <https://doi.org/10.3390/w14132126>

Academic Editors: Cheng-Yu Ku, Frank Tsai and Zheng-Yi Feng

Received: 28 April 2022

Accepted: 23 June 2022

Published: 4 July 2022

Publisher's Note: MDPI stays neutral with regard to jurisdictional claims in published maps and institutional affiliations.



Copyright: © 2022 by the authors. Licensee MDPI, Basel, Switzerland. This article is an open access article distributed under the terms and conditions of the Creative Commons Attribution (CC BY) license (<https://creativecommons.org/licenses/by/4.0/>).

1. Introduction

Many large reservoirs in southwest China have been affected by the toppling deformation bank slope stability problem, and recent studies have shown that it entails a key engineering geological problem in hydropower construction projects in southwestern China such as complex geological genetic and failure models [1–4]. There has been much research on the toppling slopes, mainly focusing on the geological mechanism [5,6], and some on the stability evaluation of and treatment measures for excavation slopes [7–13]. While these research results provide an analytical basis for the formation and distribution of toppling deformation bodies, there has been a lack of research on the influence of reservoir water impoundment on the failure process. Although some literature highlights that calculation methods of toppling failure mainly consider the toppling–sliding slope, they rarely involve toppling–bending failure [14–19]. The present analysis and evaluation of the stability of toppling deformation rock slopes mainly fall into the following categories: (1) numerical analysis methods used to analyze the deformation of toppling rock masses under external actions [20–25]; (2) limited equilibrium calculations based on block theory, such as the unbalanced thrust transfer coefficient method, the Sarma method, analytical methods and key block theory [26–29]; (3) physical simulation used to study the mechanism and process

of slope collapse [30]; and (4) uncertainty analysis and engineering geological analogy methods [31,32]. Reservoirs created by dams can affect the stability of bank slopes [33]. The impoundment of the reservoir changes the boundary condition of bank slopes and alters the stability of the reservoir slopes [34–36]. Landslides associated with reservoir impoundment have been reported widely [37]. However, there are few reports on the failure processes and the hydrodynamic effects on the failure mechanism of the toppling deformation body in the process of reservoir impoundment.

At present, a large number of scholars have carried out research on the influence of water on slope stability [38–40]. It is mostly studied from the action of saturated or unsaturated seepage force, the changes in pore pressure and the softening effect of water on rock mass [41–44]. The pore pressure and seepage pressure increase gradually as water infiltrates into the slope, and eventually lead to bank slope failure [45,46]. However, the mechanism of the influence of water on the stability of bank slope toppling deformation is rarely studied. Due to a large number of relaxation tension cracks in the toppling deformation bodies, the splitting effect of water on the rock mass accelerates the deformation of the toppling body in the process of reservoir water storage, which often exceeds the seepage and softening effect. Meanwhile, the effect of wave impaction on bank slopes after reservoir impoundment has been recognized by a large number of scholars [47–52].

In this paper, a large number of different toppling degree bank slopes along the Miaowei Hydropower Station reservoir bank were considered for the research, defining the toppling rock mass as the first failure caused by dynamic geological process and the further failure under the action of reservoir water storage or slope toe excavation as the second failure. The main objectives of the present research are as follows: (i) to develop a classification method of toppling deformation bodies; (ii) to reveal the second failure mechanism of different toppling types under reservoir water impoundment and different lithologies; and (iii) to propose a secondary failure prediction model of toppling deformation bodies after water storage. This study contributes to a more comprehensive understanding of the toppling failure mechanism in mountainous reservoirs.

2. Materials and Methods

2.1. Research Site Description

(1) The lithology of the bank slope

The bedrock strata in the reservoir area are composed of Mesozoic, Jurassic and Cretaceous strata. The Quaternary loose accumulation layer is mainly distributed at the foot of the bank slope, branch gully and valley terrace. Jurassic (*J*) strata are widely distributed along the Lancang River and are among the most important lithologies in the reservoir area. The basic geological conditions for the development of toppling rock mass were obtained by field investigation.

(2) The geological structure in the reservoir area

The reservoir is located east of the Lancang River fault zone and south of the Shideng middle-row complex anticline, which is dominated by steep vertical folds.

(3) The distribution of toppling deformation bodies in the reservoir area

Both sides of the reservoir are composed of Mesozoic strata of layered soft and hard-rock masses, and toppling deformations are relatively serious. The layered oblique (transverse) structural slope accounts for 32.8% of the bank length and 74.6% of the slope length of the bedrock bank, which is mainly distributed on both sides of the oblique valley and the transverse valley. The toppling deformation slope is distributed on both sides of the longitudinal valley.

There are 24 toppling deformation bodies in the reservoir bank area based on field investigation, mainly distributed within 1.5 to 54.6 km of the dam (Figure 1). The river has a north–south orientation with multiple bends, and there are gullies and tributaries on both sides of the river. A total of 20 toppling deformations are located on the right bank, and 4 are located on the left bank.

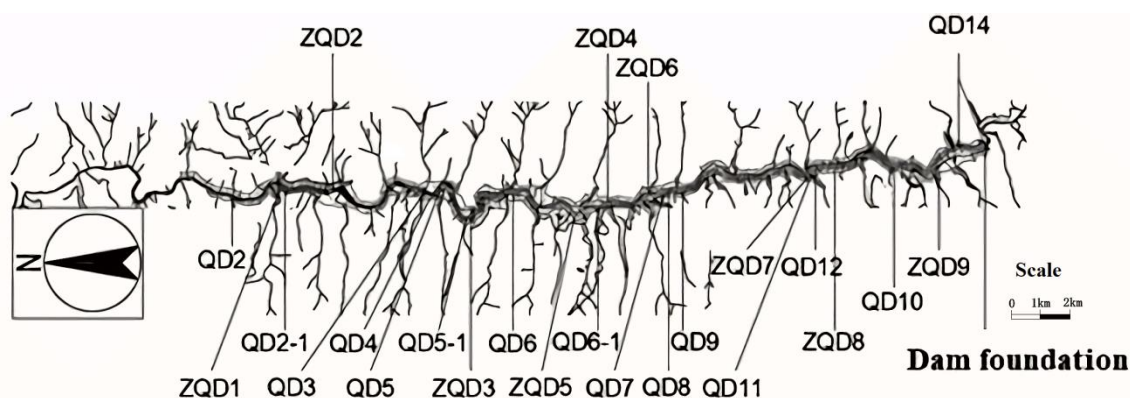


Figure 1. The distribution of toppling deformation body locations in the reservoir area.

2.2. Methodology

2.2.1. Geological Survey and Analytical Analysis

Miaowei Reservoir began to store water in November 2016, with an initial water level of 1314 m (water depth is about 10 m). Before the impoundment of the reservoir, a detailed geological survey was carried out on the bank of the reservoir. After that, in the different stages of the water level rise, unmanned aerial vehicle aerial photography and local geological surveys were used to carry out deformation observations on the toppling bank of the reservoir. Research work on the characteristics of toppling deformations includes investigating the lithologies and lithologic combinations; measuring the thicknesses of the single layers of rock, deformation degree (dip angle α ($^{\circ}$), maximum crack opening s (mm), opening angle of tension fracture, length of tension fracture), distribution of rock structural planes and the combination of the rock formations; and systematically analyzing the rock structures of toppling deformation bodies. The relationships between the changes in reservoir water level, lithology, toppling degree and the failure range and the depth of the failure surface were established using statistical analysis and engineering geological system analysis methods.

2.2.2. Field Penetration Test of Toppling Deformations

In order to study the hydrodynamic characteristics of different toppling deformations in the process of reservoir impoundment, penetration tests were performed in different types of toppling deformations: QD3, ZQD3, ZQD4, QD6-1, and QD14. The range of horizontal and vertical saturated zones under the action of the reservoir water was determined by measuring the permeability coefficient with time under different occurrences and different joint distribution characteristics of the four types of toppling deformations. The tests adopted a single-ring injection test method. The tests consisted of two types: a vertical penetration test and a horizontal penetration test. During the vertical penetration test, the depth of the water was kept at 10 m, with no more than 0.5 cm of fluctuation. During the horizontal penetration test, the initial water level, measurement time and drop height were recorded until the water level was 0.0 m or no longer falling.

By recording the water injection per unit time and the area of a single ring, the hydraulic conductivity k can be calculated according to Darcy's law:

$$k = \frac{Q}{AI} \quad (1)$$

where k is the hydraulic conductivity, cm/s; Q is the water injection per unit time, L; A is the area of the ring or the pit side area, cm^2 ; and I is the hydraulic gradient, which is dimensionless.

2.2.3. Numerical Simulation Method

The discrete element method was widely used to simulate the influence of layers and joints on rock deformation. In recent years, it has been widely used in the research on toppling deformation mechanisms [53–55]. In this paper, the influence of hydrodynamic affection on second toppling failure at different water storage levels was numerically simulated using the discrete element method. In the numerical model, the water saturation of rock mass below the water level, the decrease of mechanical properties, the pore water pressure between joints and the hydrostatic pressure on the toppling slope deformations were considered.

The discrete element method (DEM) was first proposed by Cundall for analyzing the deformation, movement trends and rigid or deformable block separation of discrete media [56]. Discrete element method is a numerical method that is suitable for studying and analyzing the stability of discontinuous rock slope. In this paper, the Universal Discrete Element code (UDEC) developed by Itasca Company is used to analyze the stability of the bank toppling slope in the reservoir area, which can effectively analyze the deformation and failure process of the bank toppling slope with discontinuous structures such as cracks and joints.

The reservoir water level outside the slope is set as a gradient every 10 m in the vertical direction; that is, 9 reservoir water levels are set at the elevations of 0 m, 10 m, 20 m, 30 m, 40 m, 50 m, 60 m, 70 m and 80 m to analyze the deformation characteristics of toppling slopes with different lithologic combination, and 10 m is the initial water level. The model height is 100 m, and the horizontal length is 170 m (Figure 2a). The constitutive model of rock mass adopts Mohr Coulomb material, and the yield criterion follows the Mohr Coulomb yield criterion. The bottom of the model was set as the velocity and displacement constraints in the vertical direction (Y direction) and the velocity and displacement constraints in the horizontal direction (X direction) of the left and right boundaries. The groundwater seepage mode is set as transient steady flow, and seepage is only formed between joints and layers. The pore water stress is determined by the elevation difference between the calculation point and the groundwater level. The model contains five strata (Figure 2b), where A is a toppling–collapse area, B1 is a toppling–loose area, B2 is a toppling–relaxation area, C is a toppling–creep area and D is intact bedrock. The physical and mechanical parameters used in the calculation are shown in Tables 1 and 2. These parameters are obtained through physical tests and engineering analogy methods. The modeling steps are shown in Figure 2c.

Table 1. The physical and mechanical parameters of rock mass.

Rock Mass	Natural Bulk Density (kN/m ³)	Saturated Bulk Density (kN/m ³)	Young's Modulus E (GPa)	Poisson's Ratio μ	Shear Strength			
					Natural Condition		Saturated Condition	
					c' (Mpa)	φ'	c' (Mpa)	φ'
Strongly weathered slate	22.0	23.5	1	0.32	0.55	26.6	0.50	21.8
Weakly weathered slate	23.5	24.5	1.6	0.30	0.60	26.6	0.48	21.8
slate	24.5	25.0	2.0	0.30	0.68	35.0	0.56	31.0
Strongly weathered metamorphic sandstone	25.0	25.5	4.0	0.30	0.70	38.7	0.57	35.0
Weakly weathered metamorphic sandstone	26.0	26.5	8.0	0.28	0.80	45.0	0.64	38.7
Metamorphic sandstone	26.5	27.0	16.0	0.25	0.90	50.2	0.80	45.0

Table 2. The mechanical parameters of joints.

Joints	Normal Stiffness (GPa/m)	Tangential Stiffness (GPa/m)	Shear Strength (Natural Condition)		Shear Strength (Saturated Condition)	
			c' (MPa)	f'	c' (MPa)	f'
Joint surface	1.0	0.4	0.10	0.50	0.05	0.50
Strongly weathered layer	1.0	0.4	0.10	0.40	0.07	0.36
Weakly weathered layer	1.5	0.8	0.30	0.55	0.21	0.50
Slightly weathered layer	2.0	1.0	0.40	0.65	0.28	0.60
Unweathered layer	5.0	2.0	0.75	1.00	0.50	0.85

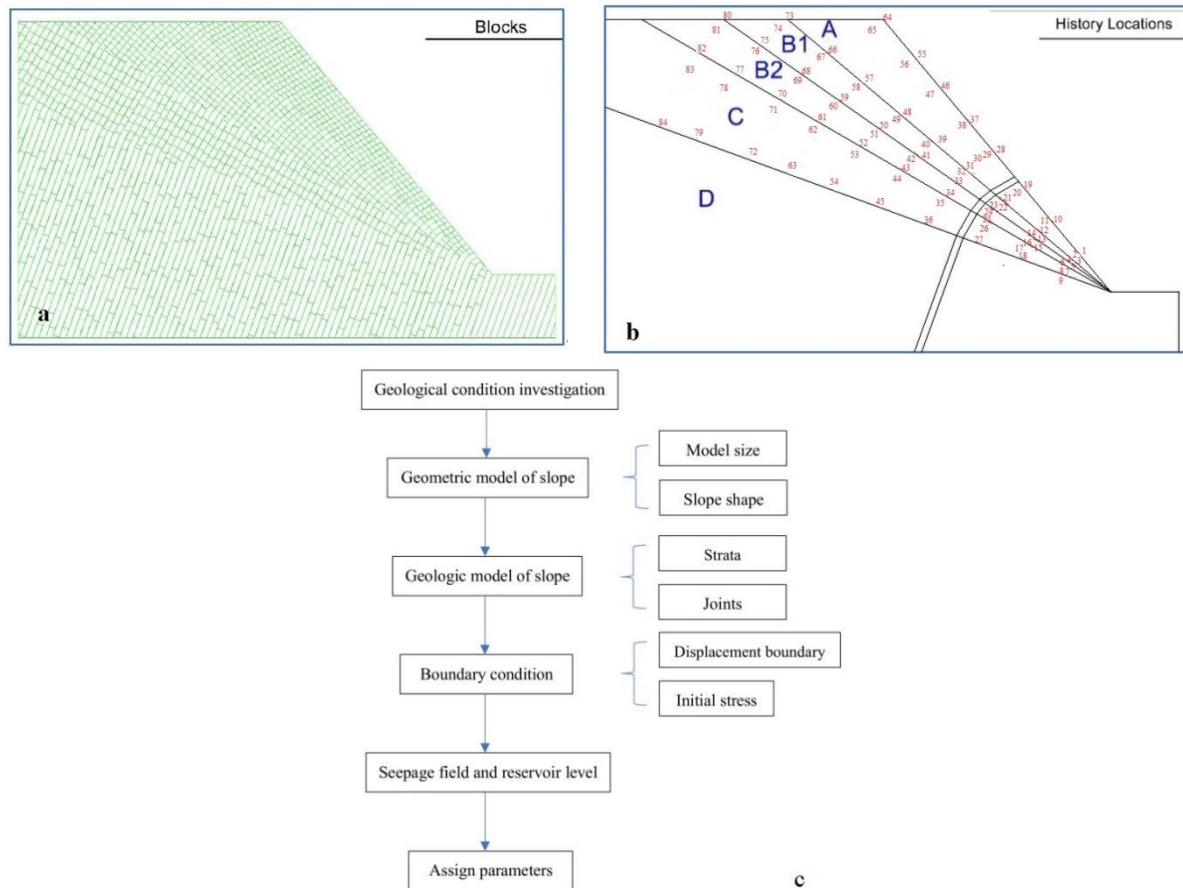


Figure 2. The calculation model and monitoring point. (a) The geometric model. (b) The monitoring point. (c) The flow chart of the modeling.

3. Results and Discussion

3.1. Distribution Characteristics of Toppling Deformation Body

The depth of the horizontal toppling influence in the local bank slope is more than 50 m, and it tends to gradually deepen with increasing elevation, which has a greater impact on the stability of the bank slope and the choice of reinforcement measures.

3.1.1. Distribution Characteristics of Left and Right Banks

The toppling deformation body distributions throughout the reservoir area are related to the topography and geomorphology, stratigraphic lithology, bank slope rock mass structure and mechanical properties of the rock masses in the area. Mostly, the direction of in situ stress plays an important role in toppling. Using the distribution map of the main tributaries in the reservoir area, the rivers noticeably deviate when they are close to entering the Lancang River, and the left-bank tributaries extend mostly in the NNW direction (upstream direction), while the right-bank tributaries extend mostly in the SSE

direction (downstream direction), indicating that during the process of entrenchment in the Lancang River valley, both sides are subjected to dual forces: The lateral stress downstream is larger than the upstream stress in the left bank, the upstream stress is larger than the downstream stress in the right bank, and rock mass toppling upstream is greater than that downstream in the right bank.

On the right bank, the toppling degree of the rock mass on the upstream side of the gully is significantly higher than that on the downstream side (Figure 3a,b), but on the left bank, the toppling degree on the downstream side is greater than that on the upstream side (Figure 3c,d).



Figure 3. (a) The toppling deformation body of the upstream side of the Keli River on the left bank. (b) The toppling deformation body of the downstream side of the second gully at the dam on the left bank. (c) The toppling deformation body of the upstream side of the Tiemenka River on the right bank. (d) The toppling deformation body of the downstream side of the Tiemenka River on the right bank.

3.1.2. Distribution Characteristics with Different Bank Slope Structures

On dip slopes, toppling often develops; the surface of the bank slope is covered with toppling–collapse rock masses, with toppling–relaxation rock masses underneath, and toppling–loose rock structure types are often missing (Figure 4a). The depth of the broken zone is generally 5–10 m below the surface, with a maximum depth of 20 m. The toppling collapse develops a relatively high elevation of 50–100 m above the river surface and is related to the stresses that the elevation underwent and the thickness of the upper accumulation terraces. There are three typical fracture-type toppling deformation profiles on the dip slope in the reservoir area (Figure 4a,b,e). Most of them are thin-layered slate, with thin 1 mm–2 cm interlayers of siltstone (Figure 4c,f). As the elevation increases, the

fracture surface approaches closer to the ground. The inclination angle of the fracture surface is approximately $20\sim 30^\circ$, which shows a gentle inclination angle (Figure 4d).



Figure 4. (a) Metasandstone toppling deformation at Qingcaiping on the left bank. (b) toppling shallow broken in metasandstone. (c) toppling broken face in consequent slope. (d) toppling broken face in reverse slope of metasandstone. (e) toppling bending in slate. (f) slate toppling deformation body at the crossing road downstream of Biaocun town on the right bank.

The depth of the toppling broken surface of the typical reverse slope in the Miaowei Reservoir area is greater than that of the dip slope, usually $15\sim 30$ m. The inclination angle of the toppling broken surface is related to the lithology of the toppling deformation body. Generally, the harder the rock is, such as that in the bank slopes dominated by metamorphic quartz sandstone, the steeper the inclination angle of the toppling broken surface, usually between $40^\circ\sim 55^\circ$. The bank slope composed of thin layers of metamorphic sandstone has an inclination angle of $30^\circ\sim 40^\circ$. On the bank slope mainly dominated by slate, the inclination angle of the slope is below 30° . From top to bottom, the orientation of the rock layer changes from $260^\circ\angle 20^\circ\sim 260^\circ\angle 40^\circ$ to $252^\circ\angle 55^\circ\sim 252^\circ\angle 84^\circ$. The lower bedrock is relatively complete, and the thickness of the crushed rock body above the broken surface is approximately 15 m (Figure 5a). The broken surface of the toppling deformation in the reverse slope is not a plane but a curved surface related to the elevation and the strength of the rock mass. The inclination angle of the broken surface increases with increasing distributed elevation (Figure 5b). Taking thin-layered metamorphic sandstone with slate as an example, the angle of the broken surface is basically $60\sim 70^\circ$ in the reverse slope toppling deformation body above the altitude of 1430 m (Figure 5c), and the angle is usually $30\sim 40^\circ$ between the altitudes of 1380 and 1430 m. This angle shows that the gravity of the upper rock mass promotes the bending broken structure of the lower rock mass.



Figure 5. (a) The angle of the toppling fracture surface is less than 10° in the reverse slope. (b) The change trend of the dip angle of the rock layer. (c) The dip angle of the toppling broken failure surface is 63° above the altitude of 1430 m. (d) The toppling-loose rock mass of the old highway slope on the downstream side of the Wanba River. (e) The toppling-relaxation rock mass of QD5-1 in the transversal.

Due to the restriction of the cutting depths of the gullies, the toppling direction of the transverse slope points upstream or downstream, and the deformation degree is light. For example, on the old highway slope on the downstream side of the Wanba River, the bedrock orientation is $N15^\circ W, NE\angle 89^\circ$, the lithology is medium-thick-layered metamorphic quartz sandstone, the rock strata are stable and the upper part is toppling toward the surface. After the toppling, the orientation of the rock layer turned to $N10^\circ W, SW\angle 43^\circ$, and the rock formation was curved in a spine shape (Figure 5d) but not buckled, forming a toppling-loose structure (Figure 5e). However, the deformation is still dominated by toppling-bending and toppling-creep structures.

3.1.3. Degree of Toppling Deformation with Different Lithology

The rock structure is mainly characterized by combinations of lithology. The degree and development depth of the toppling deformation of bank slopes with different rock structures are different. (1) For the slate-dominated bank slope, the rock mass has obvious rheology and can produce large deformation; (2) for the metamorphic sandstone-dominated bank slope, the rock mass has a certain capacity to accumulate deformation. When the accumulated stress exceeds the tensile strength or flexural rigidity of the rock mass, the rock mass first has flexural deformation and tension fracture, and the main blocks between the tensile fractures are rotated with the increase in stress in the later stage. (3) For the bank slope composed of interbedded slate and sandstone, the rock mass collapses in the form of a composite beam, and the deformation degree is controlled by the layer thickness ratio. The metamorphic sandstone is mainly broken and destroyed and separated from the top surface, forming blocks that by gravity act on the underlying slate, producing a transverse bending action on the slate, which further causes the bending deformation of the slate. The macroscopic characteristics are that the sandstone is block-shaped and the slate is curved and deformed.

3.2. Types of Toppling Deformation on the Bank Slopes

3.2.1. Severity of Toppling Deformation

The on-site investigation of the toppling deformation bodies shows that the toppling deformation rock masses in the reservoir area are composed of slate, schist, and metamorphic quartz sandstone. The toppling deformation and fracture phenomena of the rock bodies are intricate and complicated, and there are large differences in the deformation and formation mechanisms of different parts. To ascertain the deformation and fracture forms, the generation mechanisms of the rock masses at these parts, and their relationship with the intensity of rock mass toppling deformation, the following four parameters are used to objectively reflect the intensity of rock mass toppling deformation.

(1) The curvature coefficient $1/R$, an index to measure the degree of bending deformation of the rock layer, refers to the maximum radius of the rock layer that bends from the normal occurrence of the rock layer to the slope surface and is the reciprocal of the radius of curvature. For plastic rock masses, the radius of curvature is large. Different structure types of rock masses have different radii of curvature. The bank slopes dominated by thin slate rocks are prone to bending deformation, and the radius of curvature is small, while the bank slopes dominated by metamorphic sandstone have greater bending stiffness, and the curvature radius is larger.

(2) The rotation angle, the difference between the inclination angle of the toppling rock layer and the original rock, can distinguish the degree of rock layer toppling. On the same slope, different toppling deformation zones can be divided by the rotation angle, and the different toppling deformation zones have different forms of rock failure.

(3) Toppling tension cracks are generated perpendicular to the layer after the rock layer is toppled and deformed. Such cracks have the characteristics of an inverted triangle.

(4) Tensile fracture connectivity is the connectivity of the toppled deformed rock mass on its tensile fracture surface. The severity of the toppling deformation type is listed in Table 3.

Table 3. Classification of the rock toppling deformation degree.

Severity of Toppling	Curvature Coefficient	Dip Angle Rotation Ratio	Spacing of Toppling Tension Cracks (cm)	Connectivity of Tension Fracture	General Features
Toppling broken	>0.7	<0.25	<10	>80%	The rock stratum rotates obviously with obvious bending fracture zone and deformed rock mass is broken
Toppling tension	0.3~0.7	0.25~0.50	10~30	60~80%	The rock stratum rotates to a certain extent, the tension crack is discontinuous, and the deformed rock mass is relatively broken
Toppling bending	0.1~0.3	0.50~0.75	30~50	40~60%	The tensile fracture of rock is discontinuous, and the deformed rock mass is relatively broken
Toppling creep	<0.1	>0.75	>50	<40%	The dip angle of the stratum changes greatly, the plastic continuous deformation is dominant, and no discontinuous fracture occurs

3.2.2. Classification of the Toppling Deformation Rock Mass

The quality of the toppling deformed rock mass is related to the degree of toppling deformation, the spacing of structural planes, the thickness of a single layer and lithology. According to the toppling deformation degree evaluation index, the toppling deformation rock mass can be divided into four types: toppling collapse, toppling loose, toppling relaxation and toppling creep. The properties of the different toppling deformation rock masses are listed in Table 4.

Table 4. Types of toppling deformation rock masses in the reservoir area.

Types	Degree of Toppling Deformation	Characteristics of Deformation	Distribution and Lithology
Toppling collapse	toppling broken	strongly toppled off and broken, and the overall tension is loosened. The rotation angle is greater than 50°.	It is mainly distributed on the surface of the slope and has a limited distribution range. Lithology is thin-layered slate and thousand-shaped slate, mainly soft rock.
Toppling loose	toppling tension	strongly toppled and broken, and the overall rock mass is loose and partially elevated. The rotation angle is 30–50°.	It is distributed on the shallow surface layer of the slope, and the cover thickness is relatively small, generally about 1 m–3 m. The lithology is mainly thin-layered to middle-layered metamorphic sandstone, sand slate or sandstone and interbedded with slate.
Toppling relaxation	toppling bending	gently toppled, and the local fracture of the rock mass develops perpendicular to the stratum, with an opening width of about several millimeters. The rotation angle is 10–30°.	It is distributed above the toppling creep rock mass. The lithology is mainly quartz sandstone, metamorphic sandstone, etc.
Toppling creep	toppling creep	weak toppling deformation, and the rock mass within the layer has a slight tensile cracking deformation. The rotation angle is less than 10°.	The degree of toppling is weak, mainly occurring in the deep part of the slope.

3.3. Second Failure Mechanism of the Toppling Bank Slope with Reservoir Impoundment

Different toppling type slopes have different failure mechanisms; some researchers have found that the tensile strength reduction is insufficient to produce toppling as this failure mechanism starts with sliding between the layers [57,58]. For soft-hard interbedding layered slopes, however, the toppling slope failure mainly occurs as collapse under tension strength reduction. From the failure characteristics, the toppling bank slope was affected by the softening strength of the foot of the slope, wave erosion, and rainfall infiltration on the slope. When the water-storage level was raised by 50 m, the failure surface of the toppling deformation body often occurred at the interface between the toppling–collapse and toppling–loose surfaces. If the underwater depth of the bank slope exceeds 50 m, the failure surface is inside the toppling–loose rock mass. At the same time, the toppling deformation of the rock mass has time-dependent deformation characteristics. Different bank slopes in the reservoir area are affected by local stresses (such as slope height, topographical slope, unloading stress) and the structure of the bank rock mass, resulting in different degrees of development of the toppling rock mass on the bank slope. Some bank slopes have only toppling–creep rock masses, which are determined by the stage of the development of toppling deformation.

(1) Relationship between the height of the rising water level and toppling deformation body failure

It can be seen from the relationship between the underwater depth of the bank slope and the degree of failure of the toppling deformed rock mass that after the underwater depth of the bank slope of the toppling deformed rock mass reached 45 m, deformation and destruction began to occur (Figure 6a). When the storage level reaches a certain height, it will induce the occurrence of toppling deformation, and Figure 6a shows that when toppling deformation occurs, the water level generally reaches more than 45 m. The underwater depth reached 60 m–90 m, and the toppled deformed rock mass exhibited different degrees of shear tension failure.

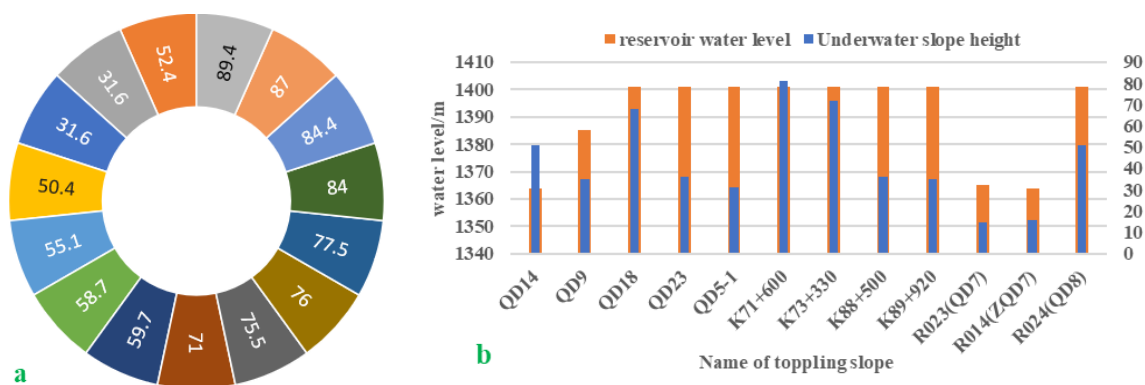


Figure 6. (a) Water depth on the front of the slope with toppling failure. (b) The relationship between the water depth in front of the slope and the quantity of toppling failure.

During the impoundment of the reservoir, secondary failure of the toppling deformation rock mass occurred on the bank slope. According to the relationship between the toppling body failure and the water depth on the slope observed in the three stages of reservoir impounding, the bank slope failure of the toppling deformation body mostly occurs when the water depth on the slope exceeds 50 m (Figure 6b).

(2) Relationship between the secondary failure of the toppling deformation body and lithology

The results of the on-site geological investigation show that the softening of the toppling deformed rock mass in the reservoir water-storage process is the main internal cause of the secondary failure of the toppling deformed masses. The bank slopes of the collapsed deformed bodies are mostly a combination of thin-layered slate and thin-layered metamorphic sandstone. Due to the fast softening of the slate, the strength of the slate that has been toppled and broken will decrease by 50% after only one week during the water-storage process and by 70% after one month. In the toppling-loose rock mass, toppling tension fractures develop. Although the fracture surface does not form a unified failure surface, the fractures have a high connectivity rate, are saturated with water and soften faster. After the reservoir has been impounded for a certain period of time, it is affected by the toppling-collapse rock mass outside the bank slope, and then the failure of the toppling-loose rock mass continues.

The softening rate of the soft rocks is obtained by testing the point load strength reduction value of rocks after water immersion softening. According to the results of laboratory tests, the strength softening rate of the soft rocks reached 28.81% after 28 days saturation (Figure 7a), and the level in the hard rocks after 28 days saturation was 25.51% (Figure 7b). Due to the structural characteristics of the toppling deformed rock mass, the reservoir water seepage rate is fast, and the slope below the water-storage level is quickly saturated. With the increase in the water level, the toppling deformed rock mass at the foot of the slope lost its strength after softening.

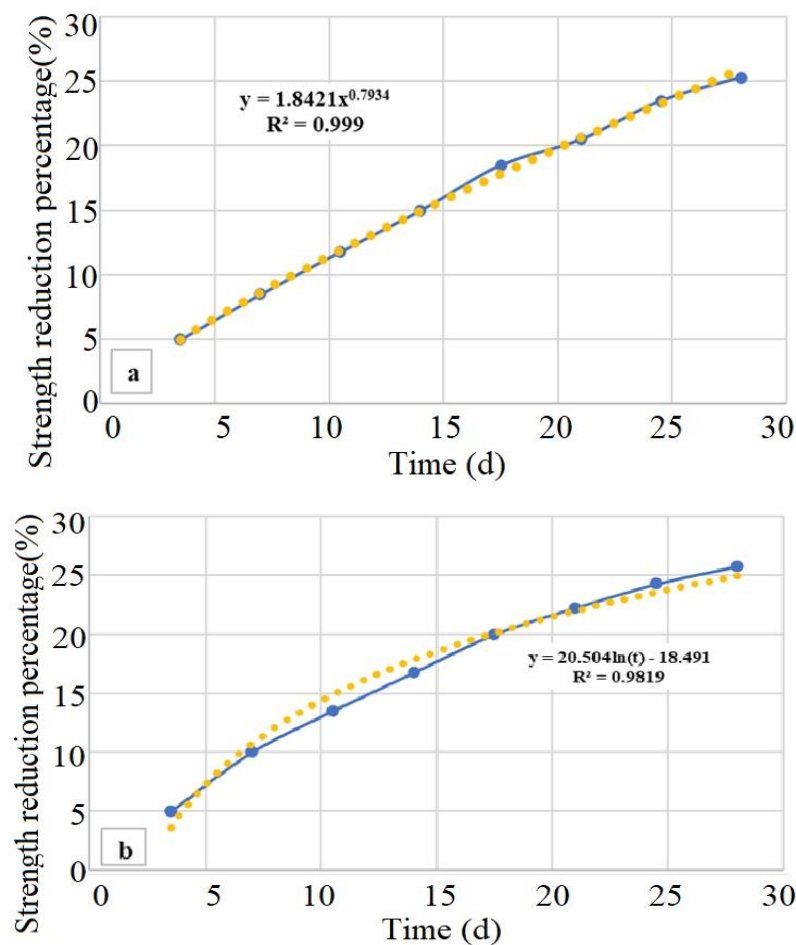


Figure 7. Reduction rate of tensile strength. (a) Metamorphic quartz sandstone and (b) slate.

(3) Hydrodynamic force affection on the collapse of toppling bank slope

In order to analyze the mechanism of hydrodynamic force on the secondary failure of toppling deformation body, the discrete element numerical simulation method was used to simulate the deformation characteristics of toppling rock mass under the action of pore water pressure in different impoundment stages. In the numerical model, the vertical and horizontal permeability coefficients of different toppling types were used based on Formula (1). The total displacement of interbedded toppling slope without water storage and water storage at 30 m, 60 m and 80 m are shown in Figure 8a–d. Before water storage, the slope forms a deformation area with a maximum displacement of 60 mm in areas B1, B2 and C, and the overall deformation is small. The deformation mainly comes from the toppling–collapse and toppling–loose areas and the closed deformation of the rock layer and joint surface. With the rise of water level, the displacement of each area increases obviously, an obvious displacement differentiation zone is generated between area A and area B, and the differentiation surface is in a slip arc shape. At the same time, an obvious displacement differentiation zone is also formed between area B2 and area C. When the storage water level reaches 60 m, the deformation of each part of the rock mass in area A exceeds 1.00 m. The deformation gradient of in area B is obvious, finally reaching 20~80 cm. The maximum displacement in area C is less than 20 cm. Accelerated deformation occurs in area A after 10 m of water storage. The deformation of rock mass below 10 m increases slightly with the rise of water level, and the displacement of the slope top finally reaches 60~100 cm (Figure 8e). Area B2 and area C deform after 10 m of water level, and the displacement in X direction of area B finally reaches 15~50 cm (Figure 8f).

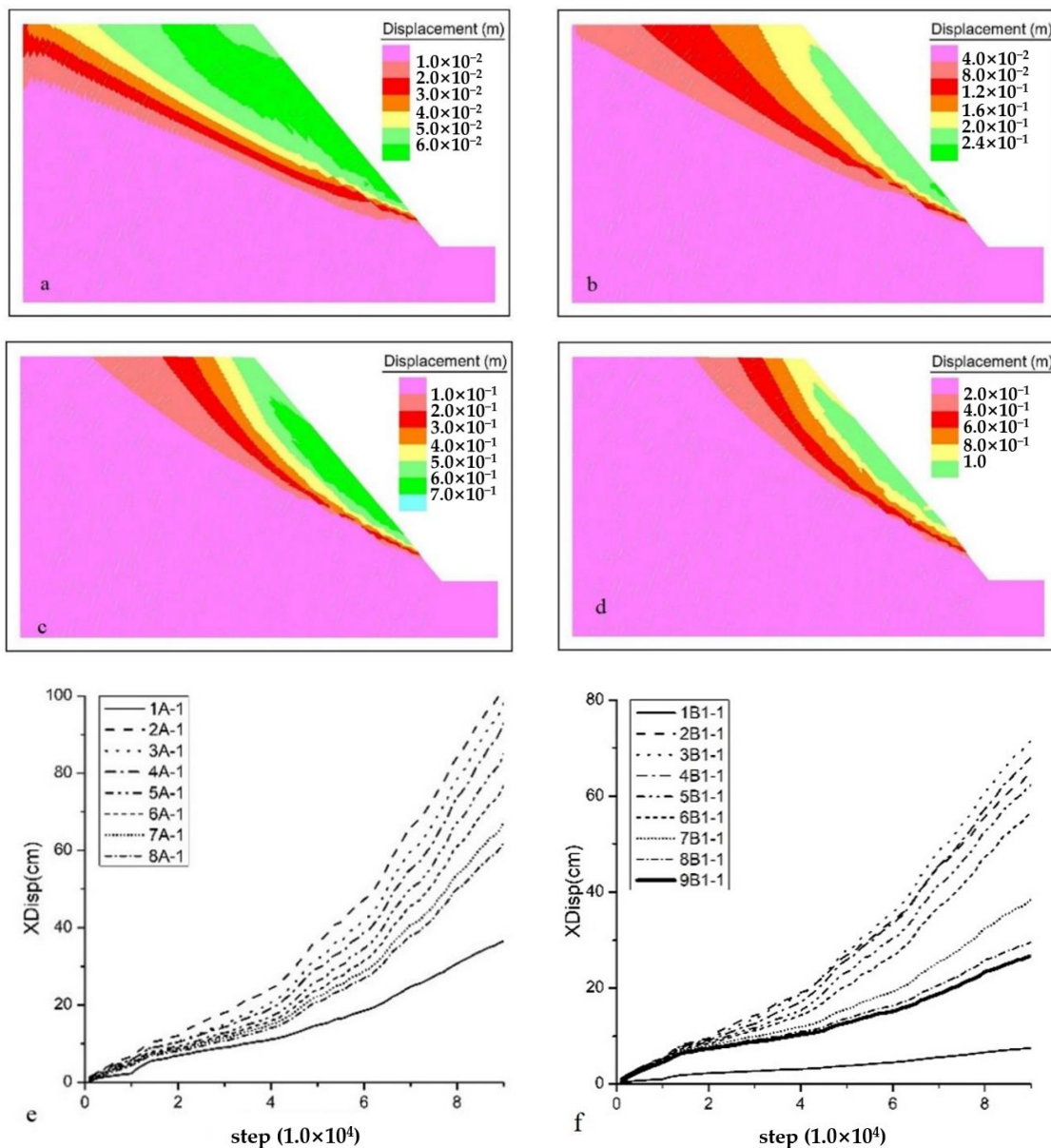


Figure 8. (a) The total displacement of slope before water storage. (b) The total displacement of slope when the reservoir impounded 30 m. (c) The total displacement of slope when the reservoir impounded 60 m. (d) The total displacement of slope when the reservoir impounded 80 m. (e) The displacement in X direction of series monitoring points in area A. (f) The displacement in X direction of series monitoring points in area B.

The numerical analysis results show that the saturated metamorphic quartz sandstone in the toppling collapse zone A is broken and sheared, while the saturated slate is squeezed to produce compression deformation. The shear failure of the lower saturated hard rock in area B1 is relatively strong. After the impoundment of the reservoir, the pore water pressure increases in the relaxation tension, promoting the development of the deformation and the failure of the slope. Approximately 90% of the toppling bank slope failure occurred within 30 days after the reservoir impoundment in the Miaowei Reservoir. At this stage, the reservoir water supplies groundwater and flows from the bank to inside the slope. Due to the development of the toppling tension fracturing of the bank slope, the seepage mode of the groundwater is a transient and steady flow, and seepage is formed only between the joints and the rock layer surface. The dynamic seepage pressure has little impact on the groundwater level of the bank slope. The main effect of the reservoir water on the bank

slope of the toppling rock mass is the increase in pore water pressure in the bank slope rock mass and the weakening effect of the rock bank slope caused by the splitting effect of the water on the existing fissures.

3.4. Prediction Model of Toppling Deformation under Reservoir Water Storage

3.4.1. Prediction Model of the Spatial Failure Range of Toppling Deformation Bodies

According to the failure stage and failure mode of the toppling rock mass in the water-storage process in the Miaowei Reservoir area, the failure of the toppling deformed rock mass on the bank slope during the impounding process occurs in stages. In general, during the water-storage process, the toppling-collapse rock mass was first damaged, and then the toppling-loose rock mass was damaged. This process is mainly affected by the severity of the toppling deformation, the underwater depth, the structural characteristics of the rock mass, the width of the water surface, the height of the slope and the slope dip. Therefore, the prediction model of the toppling slope second failure during water storage requires comprehensive consideration of the above factors.

According to the failure results of the toppling rock mass during impoundment, the ratio of the thickness of the slate and the ratio of the underwater slope height to the total slope height in the underwater bank slope are very significant (Figure 9a). The relationship of failure is expressed by the failure index λ .

$$\eta_1 = \frac{\Delta H}{H} \tag{2}$$

$$\eta_2 = \frac{\sum h_{si}}{h} \tag{3}$$

$$\lambda = \eta_1 \eta_2 / [BT] \tag{4}$$

where ΔH is the underwater slope height (m), H is the total height of the toppling rock slope (m), $\sum h_{si}$ is the total thickness of the slate or phyllite in the slope below the reservoir water level, h is the total thickness of the slope rock below the reservoir level and $[BT]$ is the fracture resistance quality index of the bank slope rock mass, which is determined by Equation (5).

$$[BT] = \sigma_{rt} k_v \tag{5}$$

where σ_{rt} is the bending strength of the rock mass (MPa) and k_v is the integrity of the rock mass, which can be determined by the density of the joints J_v (Table 5).

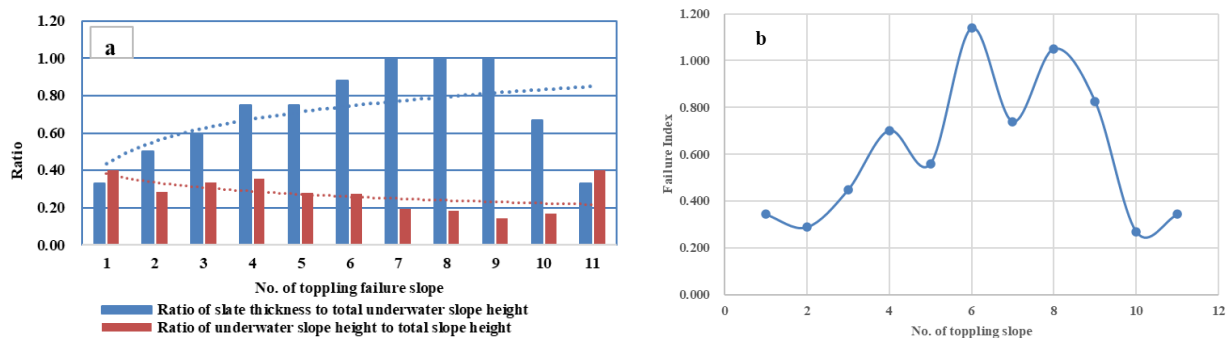


Figure 9. (a) Ratio of slate thickness to total underwater slope height. (b) Failure index λ of toppling deformation body.

Table 5. Comparison of J_v and k_v .

J_v (Joint Number/m ³)	<3	3~10	20~35	>35
k_v	>0.75	0.75~0.55	0.35~0.15	<0.15

For the toppling–collapse rock mass, J_v is less than 0.15; for the toppling–loose rock mass, it is 0.25~0.15; and for the toppling–relaxation rock mass, it is 0.55~0.35. Statistics show that the failure condition of the bank slope occurs when the failure index λ is greater than 0.25 (Figure 9b).

3.4.2. Forecasting Model of the Toppling Deformation Body Failure Time under Reservoir Water Storage

The time of toppling bank slope failure is related to the lithological combination of the toppling deformation body, the thickness of the toppling sections, and the slope dip. Suppose that the average thickness of the toppling–collapse rock mass, the toppling–loose rock mass, and the toppling–relaxation rock mass are S_A , S_B , and S_C , and the hydraulic conductivities are K_A , K_B , and K_C , respectively. Therefore, the saturation time caused by the infiltration along the inclination direction of the rock formation is expressed by the following formulas:

$$T_A = S_A/K_A I \tag{6}$$

$$T_B = S_A/K_A I + S_B/K_B I \tag{7}$$

$$T_C = S_A/K_A I + S_B/K_B I + S_C/K_C I \tag{8}$$

where I is the hydraulic gradient determined by the rising rate of reservoir water storage. According to the field tests, K_A , K_B and K_C are time-dependent, and the hydraulic conductivity by the parallel and perpendicular layers on the site can be integrated into the hydraulic conductivity along the horizontal direction of the toppling deformation body (Equation (9)).

$$\vec{K}_A = \vec{K}_{AX} + \vec{K}_{AZ} \tag{9}$$

The toppling deformation slope failure is related not only to the saturation and softening of the rock mass but also to the reservoir water-storage rate and the dynamic effect of the waves on the water surface. Therefore, the time to predict the failure of the toppling deformation rock mass on the bank slope can be comprehensively determined by Equation (10). Determine the time point by determining the storage rate.

$$E_w + \sigma_t \eta \geq \sum \sigma_{ti} h_i \tag{10}$$

Because part of the rock mass at the foot of the slope is softened by saturated water and washed away by turbulence along the shore, an area cavity is formed in the lower part of the slope. When the cavity is large enough, it will cause the upper toppling rock mass to be sheared, resulting in slope failure. Suppose the height of the slope below the water-storage level is ΔH , and the height of the softening and collapse of the slope foot is $\Delta H'$. Then, the cantilever length of the toppling rock layer is $MN = L$, and the gravity of the potential damage part above the cantilever section is determined by Equation (11).

$$W = \frac{1}{2} r_w L (H - \Delta H + \Delta H') / \cos \alpha \tag{11}$$

where r_w is volumetric weight of rock (kN/m^3) and α is slope angle ($^\circ$).

The transverse bending force acting on the cantilever rock formation is: $F = w \cos \delta$. Where δ is dip angle of rock stratum ($^\circ$) and w is self weight of rock stratum (kN).

Assuming that the thickness of a rock layer above the cavity is h_i , the bending strength of this rock layer is $\sigma_{ti} h_i$, and the conditions for the rock layer to bend and break are:

$$\sigma_{ti} h_i \leq w \cos \delta \tag{12}$$

$$\sigma_{ti} = \sigma_{t0} \mu \tag{13}$$

where σ_{i0} is the initial tensile strength of the rock formation (MPa), μ is the strength reduction rate of the rock formation. The bending strength reduction rate of different rock masses is obtained through experiments.

For the bank slope formed by the combination of hard rock and soft rock, the bending strength of the rock mass can be determined by the thickness weighted average value (Equation (14)).

$$\bar{\sigma}_i = \sum_{i=1}^n \sigma_{ti} h_i \quad (14)$$

In this way, continue to calculate layer by layer until Equation (14) is satisfied, and the secondary overall failure of the toppling deformed rock mass will occur.

After the impoundment of the reservoir, traction flow occurs along the shore. It will transport the rock and soil of the bank slope that has collapsed. As a result, the disintegrating material of the bank slope is transported to form bank slope cavities. The carrying capacity of the traction flow is manifested in two aspects. One is the thrust of the fluid acting on the sediment; the magnitude of the thrust depends mainly on the flow velocity. The other aspect is the impact load; the magnitude of the load depends on the flux of the fluid. Equation (15) can be used to calculate the traction of flow along the bank.

$$P = r_w H I \quad (15)$$

The calculation formula of saturated disintegrating rock blocks in the bank slope caused by the traction of the flow is as follows:

$$p \Delta t = M \Delta V \quad (16)$$

where p is the average driving force of the turbulent flow on the block, Δt is the time, M is the mass of the pushed object determined by the size and volumetric weight of the block after disintegration and ΔV is the speed change. Assuming that the block leaves the bank slope after generating L due to the impact, then

$$\Delta V = L / \Delta t \quad (17)$$

The time required for the underwater rock mass of the slope to be transported by the flow is:

$$T_3 = \Delta t = \frac{ML}{r_w H I} \quad (18)$$

where γ_w is the volumetric weight of the water (kN/m^3); H is the water depth (m); and I is the hydraulic gradient, which is determined by the reservoir storage rate and the gradient of the riverbed upstream and downstream.

As discussed in Section 2.2, the time for the saturation of the underwater rock layer and the turbulent impact existing on the reservoir bank will form a cavity in a certain area at the slope foot. This total time is determined by Equation (19).

$$T = T_1 + T_2 + T_3 \quad (19)$$

where T_1 is determined by Equation (8), T_2 is determined by Equation (10), and T_3 is determined by Equation (18).

3.4.3. Prediction of the Toppling Bank Slope Failure Scope under Reservoir Impoundment at 1408 m

The damage range of 24 toppling deformation bodies of the Miaowei Hydropower Station under reservoir water level 1408 m was predicted (Table 6) using the above model. In the scope prediction of the second failure of the toppling bank, the position of the final failure surface needs to be determined first; this position is controlled by the depth of the broken toppling surface. Based on the combination of lithology and layer thickness, the

range of the preferential collapse area and horizontal erodible zone was calculated, and then, the corresponding calculation model was used to predict the range of damage.

Table 6. Prediction results for the final failure range of the toppling deformed bank slope under the condition of 1408-m water storage.

No. of Toppling	Buildings Affected	Lithology	Thickness Ratio (Sandstone: Slate)	Deformation Depth (m)	Prediction of Bank Collapse Height (m)	Failure Time (day)	Actual Collapse Height (m)
ZQD2	No	Slate with sandstone	1:3	30~40	42.0	24	30
QD14	Country road	Slate with sandstone	1:3	25~30	200.0	29	180
QD2	Riverside highway	Slate with sandstone	1:2	70~90	12.0	636	10
QD2-1	Riverside highway	slate	90%	80~100	13.0	627	30
QD3	Riverside highway	slate	90%	60~70	22.0	522	60
QD4	Riverside highway	slate	90%	60~70	15.0	522	35
QD5-1	Residential houses, Riverside highway	Sandstone slate interbedding	1:1	30~40	35.0	93	10
QD6	Residential houses, Riverside highway	Slate with sandstone	1:1.5	45~50	36.0	721	30
ZQD5	Residential houses, Riverside highway	Slate with sandstone	1:4	65~70	/ *	/	12
QD7	Zayang village, Riverside highway	slate	90%	50~60	140.3	320	50
QD9	Riverside highway	Sandstone with slate	2:1	30~35	160.0	320	80
QD11	Riverside highway	Sandstone with slate	2:1	30~40	/	/	10
QD12	Riverside highway	Sandstone with slate	1:3	40~45	/	/	15
ZQD7	Riverside highway	Sandstone with slate	2:1	20~25	47.0	65	15
ZQD8	Riverside highway	Sandstone with slate	3:1	20~30	49.0	90	30
ZQD9	Residential houses, Riverside highway	slate	90%	70~80	76.3	20	8
QD5	No	Slate with sandstone	1:1.5~1:2	40~50	52.0	59	30
QD8	Zayang village, Riverside highway	Slate with sandstone	1:8	40~50	56.5	52	30
ZQD1	Fengdian power station, Riverside highway	Sandstone slate interbedding	1:1	60~70	/	/	
ZQD3	Residential houses, Riverside highway	Sandstone slate interbedding	1:1	35~45	36.0	57	10
ZQD4	Keli village	Slate with sandstone	1:1.5	20~25	/	/	30
ZQD6	No	Sandstone slate interbedding	1:1	35~40	42.0	61	8
QD6-1	Riverside highway	Sandstone slate interbedding	1:1	35~45	/	/	10
QD10	Riverside highway	slate	90%	60~80	/	/	35

Note: * will not occur bank collapse.

4. Conclusions

Based on related experiments, field investigation of the toppling deformation index, analytical analysis and numerical analysis, the deformation process and the toppling rock mass is systematically analyzed, and the deformation trends of the toppling deformation masses under the reservoir water-storage condition are predicted. The scientific basis is provided for predicting the stability of bank slopes during normal reservoir operation and prevention measures. The study reached the following conclusions.

(1) The first formation of a toppling rock mass is not only the result of gravity but also the result of long-term tectonic stress. The transverse bending effect is more significant on the reverse slope; longitudinal bending is significant in the dip slope, and toppling appears only on the surface of the slope.

(2) According to the severity of toppling deformation, the toppling deformation rock mass can be divided into four types: toppling collapse, toppling loose, toppling relaxation

and toppling creep. Because the toppling–collapsed rock mass has a relatively obvious fracture surface, it has a low resistance to softening and disintegration, and the block at the foot of the slope is easily washed away and muddled. Secondary failure often occurs during the water-storage process and shortly after water storage.

(3) Tension cracks formed during the toppling deformation process create good conditions for the reservoir water to penetrate the slope. The groundwater level rises rapidly with the rise of the reservoir water level, which leads to an increase in pore water pressure and a decrease in the effective stress of the anti-sliding section, resulting in a decrease in stability. The failure of the toppling rock mass is usually due to the free face in the lower part, and the upper rock mass is in an unsupported “floating” state, resulting in the concentration of compressive stress at the topographic turning point in the middle and lower parts of the slope. Then, the deformation is transmitted upward through the misalignment, rotation, and slipping of the joints so that the upper slope is in a tensile state, which causes tensile cracks on the surface, and the upper rock mass is prone to collapse due to toppling deformation.

(4) The prediction results of different toppling deformation slopes on the Miaowei reservoir are in good agreement with the actual situation of many toppling collapses, which proves the effectiveness of the prediction model. The second failure scope and time prediction model of the toppling deformed rock mass proposed in this paper can be used to predict the toppling slope failure banks during the impounding process stages in alpine gorge reservoirs in southwest China. The results of this study are an important reference for the development of a prevention–control design of toppling and for ensuring operational safety in alpine gorge reservoir areas.

Author Contributions: Conceptualization, F.Z. and J.L.; methodology, Z.S. and F.Z.; validation, M.D., F.Y. and L.C.; formal analysis, M.D. and F.Y.; investigation, J.L. and F.Y. All authors have read and agreed to the published version of the manuscript.

Funding: This study was supported by the Key Laboratory of Coastal Disaster and Defense of Ministry of Education, Hohai University [grant number 201912]; the open fund of the State Key Laboratory of Coastal and Offshore Engineering, Dalian University of Technology [grant number LP2105] and the Science Foundation of China Huaneng Group Co., Ltd. (20158101216).

Data Availability Statement: Not applicable.

Acknowledgments: The authors express their sincere thanks to the anonymous reviewers and the editor for their invaluable help and guidance throughout this research. The author also thanks Ding Yangbo for providing relevant calculations.

Conflicts of Interest: The authors declare no conflict of interest.

References

1. Huang, R.; Yang, G.; Yan, M.; Liu, M. Engineering geology study on a large-scale toppling deformation at Xiaowan Hydropower Station. In *Landslides and Engineered Slopes. From the Past to the Future, Two Volumes+ CD-ROM*; CRC Press: Boca Raton, FL, USA, 2008; pp. 411–416. [[CrossRef](#)]
2. Gu, D.M.; Huang, D. A complex rock topple-rock slide failure of an anaclinal rock slope in the Wu Gorge, Yangtze River. *China Eng Geol.* **2016**, *208*, 165–180. [[CrossRef](#)]
3. Liu, M.; Liu, F.-Z.; Huang, R.-Q.; Pei, X.-J. Deep-seated large-scale toppling failure in metamorphic rocks: A case study of the Erguxi slope in southwest China. *J. Mt. Sci.* **2016**, *13*, 2094–2110. [[CrossRef](#)]
4. Huang, R.; Li, Y.; Yan, M. The implication and evaluation of toppling failure in engineering geology practice. *J. Eng. Geol.* **2017**, *5*, 1165–1181. [[CrossRef](#)]
5. Beichuan, H.; Sijing, W. Mechanism for toppling deformation of slope and analysis of influencing factors on it. *J. Eng. Geol.* **1999**, *3*, 213–217. [[CrossRef](#)]
6. Zhang, Z.; Wang, T.; Wu, S.; Tang, H. Rock toppling failure mode influenced by local response to earthquakes. *Bull. Eng. Geol. Environ.* **2015**, *75*, 1361–1375. [[CrossRef](#)]
7. Bobet, A. Analytical solutions for toppling failure. *Int. J. Rock Mech. Min. Sci.* **1999**, *36*, 971–980. [[CrossRef](#)]
8. Brown, A. Toppling induced movements in large, relatively flat rock slopes. In *Proceedings of the 23rd Symposium on Rock Mechanics*, Berkeley, CA, USA, 25–27 August 1982; pp. 1035–1047.

9. Qiu, J.; Ren, G.M.; Wang, Y.N. Characteristics of forming conditions and development scale of toppling in anti-dip and dip stratified slopes. *Rock Soil Mech.* **2016**, *37*, 513–524, 532. [[CrossRef](#)]
10. Goodman, R.E.; Bray, J.W. Toppling of rock slopes. In *Rock Engineering for Foundations & Slopes*; ASCE: American Society of Civil Engineers: New York, NY, USA, 1976; pp. 201–234.
11. Goodman, R.E. Toppling—A fundamental failure mode in discontinuous materials—Description and analysis. In Proceedings of the 2013 Congress on Stability and Performance of Slopes and Embankments III, Geo-Congress 2013, San Diego, CA, USA, 3–7 March 2013; Geotechnical Special Publication. American Society of Civil Engineers (ASCE): New York, NY, USA, 2013; pp. 2348–2378. [[CrossRef](#)]
12. Smith, J.V. Self-stabilization of toppling and hillside creep in layered rocks. *Eng. Geol.* **2015**, *196*, 139–149. [[CrossRef](#)]
13. Hoek, E.; Bray, W.J. *Rock Slope Engineering*, 3rd ed.; Taylor & Francis: Abingdon, UK, 1981. [[CrossRef](#)]
14. Adhikary, D.P.; Dyskin, A.V.; Jewell, R.J.; Stewart, D.P. A study of the mechanism of flexural toppling failure of rock slopes. *Rock Mech. Rock Eng.* **1997**, *30*, 75–93. [[CrossRef](#)]
15. Wang, F.; Tang, H.; Zhang, G.; Lu, X. Development Characteristics and Evolution Mechanism of the Deep-Seated Toppling in the Upstream of the Yalong River, China. *Mt. Res.* **2018**, *36*, 411–421. [[CrossRef](#)]
16. Amini, M.; Ardestani, A.; Khosravi, M.H. Stability analysis of slide-toe-toppling failure. *Eng. Geol.* **2017**, *228*, 82–96. [[CrossRef](#)]
17. Amini, M.; Ardestani, A. Stability analysis of the north-eastern slope of Daralou copper open pit mine against a secondary toppling failure. *Eng. Geol.* **2019**, *249*, 89–101. [[CrossRef](#)]
18. Xie, L.; Yan, E.; Wang, J.; Lu, G.; Yu, G. Study on evolutionary characteristics of toppling deformation of reverse-dip layered rock slope based on surface displacement monitoring data. *Environ. Earth Sci.* **2018**, *77*, 156. [[CrossRef](#)]
19. Pritchard, M.A.; Savigny, K.W. Numerical modelling of toppling. *Can. Geotech. J.* **1990**, *27*, 823–834. [[CrossRef](#)]
20. Barla, G.; Borri-Brunetto, M.; Devin, P.; Zaninetti, A. Validation of a distinct element model for toppling rock slopes. In Proceedings of the International 7th Congress of the ISRM, Tokyo, Japan, 1 January 1995; pp. 417–421.
21. Lanaro, F.; Jing, L.; Stephansson, O.; Barla, G. DEM modelling of laboratory tests of block toppling. *Int. J. Rock Mech. Min. Sci. Geomech. Abstr.* **1997**, *34*, 506–507. [[CrossRef](#)]
22. Pinheiro, A.L.; Lana, M.S.; Sobreira, F.G. Use of the distinct element method to study flexural toppling at the Pico Mine, Brazil. *Bull. Eng. Geol. Environ.* **2015**, *74*, 1177–1186. [[CrossRef](#)]
23. Zheng, Y.; Chen, C.; Liu, T.; Xia, K.; Liu, X. Stability analysis of rock slopes against sliding or flexural-toppling failure. *Bull. Eng. Geol. Env.* **2018**, *77*, 1383–1403. [[CrossRef](#)]
24. Zheng, Y.; Chen, C.; Liu, T.; Zhang, H.; Xia, K.; Liu, F. Study on the mechanisms of flexural toppling failure in anti-inclined rock slopes using numerical and limit equilibrium models. *Eng. Geol.* **2018**, *237*, 116–128. [[CrossRef](#)]
25. Babiker, A.F.A.; Smith, C.C.; Gilbert, M.; Ashby, J.P. Non-associative limit analysis of the toppling-sliding failure of rock slopes. *Int. J. Rock Mech. Min. Sci.* **2014**, *71*, 1–11. [[CrossRef](#)]
26. Mohtarami, E.; Jafari, A.; Amini, M. Stability analysis of slopes against combined circular-toppling failure. *Int. J. Rock Mech. Min. Sci.* **2014**, *67*, 43–56. [[CrossRef](#)]
27. Alejano, L.R.; Carranza-Torres, C.; Giani, G.P.; Arzúa, J. Study of the stability against toppling of rock blocks with rounded edges based on analytical and experimental approaches. *Eng. Geol.* **2015**, *195*, 172–184. [[CrossRef](#)]
28. Haghgouei, H.; Kargar, A.R.; Amini, M.; Esmaeili, K. An analytical solution for analysis of toppling-slumping failure in rock slopes. *Eng. Geol.* **2020**, *265*, 105396. [[CrossRef](#)]
29. Zambak, C. Design charts for rock slopes susceptible to toppling. *J. Geotech. Eng.* **1983**, *109*, 1039–1062. [[CrossRef](#)]
30. Majidi, A.; Amini, M. Analysis of geo-structural defects in flexural toppling failure. *Int. J. Rock Mech. Min. Sci.* **2011**, *48*, 175–186. [[CrossRef](#)]
31. Paronuzzi, P.; Rigo, E.; Bolla, A. Influence of fling–drawdown cycles of the Vajont reservoir on Mt. Toc slope stability. *Geomorphology* **2013**, *191*, 75–93. [[CrossRef](#)]
32. Luo, X.Q.; Sun, H.; Tham, L.G.; Junaideen, S.M. Landslide model test system and its application on the study of Shiliushubao landslide in Three Gorges Reservoir area. *Soils Found* **2010**, *50*, 309–317. [[CrossRef](#)]
33. Pudasaini, S.P. A novel description of fluid flow in porous and debris materials. *Eng. Geol.* **2016**, *202*, 62–73. [[CrossRef](#)]
34. Kafle, J.; Pokhrel, P.R.; Khattri, K.B.; Kattel, P.; Tuladhar, B.M.; Pudasaini, S.P. Landslide-generated tsunami and particle transport in mountain lakes and reservoirs. *Ann. Glaciol.* **2016**, *57*, 232–244. [[CrossRef](#)]
35. Lane, P.A.; Griffiths, D.V. Assessment of stability of slopes under drawdown conditions. *J. Geotech. Geoenviron.* **2000**, *126*, 443–450. [[CrossRef](#)]
36. Putty, M.R.Y.; Prithviraj, B.N.; Kumar, P.N.; Nithish, M.G.; Giri, G.; Chandramouli, P.N. An insight into the hydrological aspects of landslides of 2018 in Kodagu, South India. *Landslides* **2021**, *18*, 1597–1610. [[CrossRef](#)]
37. Shrestha, H.K.; Yatabe, R.; Bhandary, N.P. Groundwater flow modeling for effective implementation of landslide stability enhancement measures. *Landslides* **2008**, *5*, 281–290. [[CrossRef](#)]
38. Zhang, X.; Chen, L.; Zhang, F. Impact of fluid turbulent shear stress on failure surface of reservoir bank landslide. *Arab. J. Geosci.* **2018**, *11*, 698. [[CrossRef](#)]
39. Alonso, E.E.; Gens, A.; Delahaye, C.H. Influence of rainfall on the deformation and stability of a slope in overconsolidated clays: A case study. *Hydrogeol. J.* **2003**, *11*, 174–192. [[CrossRef](#)]

40. Calvello, M.; Cascini, L.; Sorbino, G. A numerical procedure for predicting rainfall-induced movements of active landslides along pre-existing slip surfaces. *Int. J. Numer. Anal. Methods Geomech.* **2007**, *32*, 327–351. [[CrossRef](#)]
41. Cascini, L.; Calvello, M.; Grimaldi, G.M. Groundwater modelling for the analysis of active slow-moving landslides. *J. Geotech. Geoenviron. Eng. (ASCE)* **2010**, *136*, 1220–1230. [[CrossRef](#)]
42. Sun, G.; Zheng, H.; Tang, H.; Dai, F. Huangtupo landslide stability under water level fluctuations of the Three Gorges reservoir. *Landslides* **2016**, *13*, 1167–1179. [[CrossRef](#)]
43. Maihemuti, B.; Wang, E.; Hudan, T.; Xu, Q. Numerical simulation analysis of reservoir bank fractured rock-slope deformation and failure processes. *Int. J. Geomech.* **2016**, *16*, 04015053. [[CrossRef](#)]
44. Huang, Z.; Jiang, Z.; Zhu, S.; Wu, X.; Yang, L.; Guan, Y. Influence of structure and water pressure on the hydraulic conductivity of the rock mass around underground excavations. *Eng. Geol.* **2016**, *202*, 74–84. [[CrossRef](#)]
45. Pelinovsky, E.N.; Mazova, R.K. Exact analytical solution of nonlinear problems of tsunami wave runup on slopes with different profiles. *Nat. Hazards* **1992**, *6*, 227–249. [[CrossRef](#)]
46. Jiang, L.; LeBlond, P.H. Numerical modeling of an underwater Bingham plastic mudslide and the waves which it generates. *J. Geophys. Res.* **1993**, *98*, 10303–10317. [[CrossRef](#)]
47. Rabinovich, A.B.; Thomson, R.E.; Fine, I.V.; Kulikov, E.A.; Bornhold, B.D. Numerical modelling of tsunamis generated by hypothetical landslides in the Strait of Georgia, British Columbia. *Pure Appl. Geophys.* **2003**, *160*, 1273–1313. [[CrossRef](#)]
48. Fine, I.; Rabinovich, A.; Bornhold, B.; Thomson, R.; Kulikov, E. The grand banks landslide-generated tsunami of November 18, 1929: Preliminary analysis and numerical modeling. *Mar. Geol.* **2005**, *215*, 45–57. [[CrossRef](#)]
49. Lobkovsky, L.; Mazova, R.; Remizov, I.; Baranova, N. Local tsunami run-up depending on initial localization of the landslide body at submarine slope. *Landslides* **2021**, *18*, 897–907. [[CrossRef](#)]
50. Nichol, S.L.; Hungr, O.; Evans, S.G. Large-scale brittle and ductile toppling of rock slopes. *Can. Geotech. J.* **2002**, *39*, 773–788. [[CrossRef](#)]
51. Alzo'ubi, A.K.; Martin, C.D.; Cruden, D.M. Influence of tensile strength on toppling failure in centrifuge tests. *Int. J. Rock Mech. Min. Sci.* **2010**, *47*, 974–982. [[CrossRef](#)]
52. Zhang, X.; Simons, R. Experimental investigation on the structure of turbulence in the bottom wave-current boundary layers. *Coast. Eng.* **2019**, *152*, 103511. [[CrossRef](#)]
53. Spreafico, M.C.; Cervi, F.; Francioni, M.; Stead, D.; Borgatti, L. An investigation into the development of toppling at the edge of fractured rock plateaux using a numerical modelling approach. *Geomorphology* **2017**, *288*, 83–98. [[CrossRef](#)]
54. Cundall, P.A. A Computer Model for Simulating Progressive, Large-Scale Movements in Blocky Rock Systems. *Proc. Symp. Int. Soc. Rock Mech.* **1971**, *2*, 2–8.
55. Pant, S.; Adhikary, D.; Dyskin, A. Slope failure in a foliated rock mass with non-uniform joint spacing: A Comparison Between Numerical and Centrifuge Model Results. *Rock Mech. Rock Eng.* **2015**, *48*, 403–407. [[CrossRef](#)]
56. Adhikary, D.P.; Dyskin, A.V.; Jewell, R.J. Numerical modelling of the flexural deformation of foliated rock slopes. *Int. J. Rock Mech. Min. Sci. Geomech. Abstr.* **1996**, *33*, 595–606. [[CrossRef](#)]
57. Adhikary, D.P.; Dyskin, A.V. A continuum model of layered rock masses with non-associative joint plasticity. *Int. J. Numer. Anal. Meth. Geomech.* **1998**, *22*, 245–261. [[CrossRef](#)]
58. Adhikary, D.P.; Muhlhaus, H.B.; Dyskin, A.V. Modelling the large deformations in stratified media—A Cosserat continuum approach. *Mech. Cohesive-Frict. Mater.* **1999**, *4*, 195–213. [[CrossRef](#)]